Gemini surfactant abetted synthesis of mesoporous Mn/Mg bimetal doped TiO$_2$ nanomaterial: Characterization and photocatalytic activity studies under visible light irradiation

Sankara Rao Miditana
Andhra University

Siva Rao Tirukkovalluri
Andhra University

Imandi Manga Raju
Andhra University

Shaik Abdul Alim
Andhra University

Genji Jaishree
Andhra University

M.L.V. Prasanna Chippada
Andhra University

Research

Keywords: Mn2+/Mg2+ bimetal doped TiO2, Gemini Surfactant, Mehtyl Red, Mesoporous Nanocatalyst, Sol-gel technique, Anatase TiO2

Abstract

The present work mainly aimed to synthesize different weight percentages (0.25-1.00 wt%) of Manganese (Mn^{2+}) and Magnesium (Mg^{2+}) bimetal ions doped TiO_2 nanomaterial assisted with different weight percentages (5-15 wt%) of Gemini Surfactant (GS) using sol-gel method. The bimetal doped and undoped TiO_2 photocatalysts were characterized by X-ray Diffraction, Scanning Electron Microscopy, Energy Dispersive X-ray Spectroscopy, Fourier Transform Infrared Spectroscopy (FT-IR), UV-Visible Diffused Reflectance Spectroscopy, Transmission Electron Microscopy, Brunauer-Emmett-Teller surface area analyzer, and Photoluminescence Spectroscopy. Characterization results evinced that Mn^{2+}/Mg^{2+} bimetal ions doping and encapsulation of GS on TiO_2 nanoparticles promote the formation of mesoporous multi-particle anatase TiO_2 nanocatalysts with a narrowed band gap, less particle size, and high surface area. The surface elemental composition of the 0.25 wt% Mn^{2+}& 1.00 wt% Mg^{2+} bimetal doped TiO_2 in presence of 10 wt% of Gemini surfactant (after calcination) revealed the presence of both the metal dopants Mn^{2+} and Mg^{2+} along with the Ti and O and their chemical interactions were further confirmed by FT-IR results. The photocatalytic activity of these catalysts was assessed by the degradation of Methyl Red (MR) using visible light irradiation. To understand the effect of different reaction parameters on the photocatalytic activity of the nanocatalysts such as the dopant concentration, GS concentration, catalyst dosage, solution pH, and initial dye concentrations were investigated and optimized to achieve the best performance. The photoluminescence results conclude that OH radicals are the crucial reactive species responsible for oxidative photocatalytic degradation of MR.

1. Introduction

It is worth noting that among the different semiconductors that are being studied from the past few decades for the photocatalytic degradation of various organic pollutants from wastewater, TiO_2 stands as the most preferable one due to its non-toxicity, non-corrosive, photostability and low cost. To make it suitable for visible light activity, many attempts are being made to modify the TiO_2 electronic structure to overcome its disadvantages of high bandgap energy and high rate of electron-hole recombination. The recent literature findings revealed that bimetal ions doping into TiO_2 crystal lattice had overcome the above drawbacks and significantly enhanced its visible light activity [1-3]. Among the various metal ion dopants studied so far, transition metal ion dopants can greatly reduce the bad gap and electron-hole recombination by forming an extra energy level below the conduction band of TiO_2 due to the interaction of their 3d or 4d states with Ti 3d states [4]. Recently, K.V. Divya Lakshmi et al. reported that Manganese is most preferable among the transition metals owing to the presence of t_2g orbital of d is very close to the conduction band of TiO_2 by which the absorption can be possibly shifted to the visible part of the spectrum [5]. On the other hand, Changneng Zhang et al., Desta shumuye et al. and Sofiaou et al. were investigated the effect of Magnesium, an alkaline earth metal on the crystalline structure and catalytic activity of TiO_2 and found its absorption band was shifted more towards the visible region, which resulted in performing high photocatalytic activity [6-8]. Hence, Mn^{2+} and Mg^{2+} ions could be more

effective as metal ion dopants to modify the TiO_2 for better photocatalytic performance under visible light irradiation.

As the size, shape, and surface area of the photocatalyst plays a major role in the photocatalytic degradation process of organic pollutants from wastewater, surfactants were the best-reported species to control the growth and agglomeration of nanoparticles during the synthesis process. Among those surfactants, more surface-active anionic Gemini surfactant, 1,4-Butane sultone (GS) is the most suitable as a capping agent to fabricate the spherical shaped bimetal doped TiO_2 nanoparticles with small grain size and large surface area [9]. Hence, in the present study, we aimed to synthesize the Mn^{2+} and Mg^{2+} bimetal doped TiO_2 nanoparticles in the presence of Gemini surfactant using the sol-gel process through which we can achieve high purity and homogeneous materials at room temperatures under stoichiometry control [10].

Compared to bulk materials nanomaterials possesses unique physical, chemical, and mechanical properties. To understand overall properties, it is important to characterize the structural, optical, and morphological properties of nanomaterials prior to proceed for different applications to obtain better results [11]. Hence, several advanced sophisticated techniques were used in the present study to characterize the crystalline phase, surface morphology, elemental composition, visible light absorption capacity, particle size, and surface area of as-synthesized bimetal doped TiO_2 nanoparticles to understand its suitability for photocatalytic degradation applications.

Due to the widespread industrial activities, various organic dye pollutants are being discharged into water bodies causing severe water pollution. Almost, 15% of the dyes produced worldwide are lost during synthesis and processing with wastewater. Moreover, 50% of all the dyes used in various industries are carcinogenic azo dyes, which are characterized by one or more azo bonds (-N=N-) [12] among which, Methyl Red is a familiar azo dye and is widely used in paper printing, textile dyeing, and leather industries [13]. It causes skin & eye irritation and irritation of the respiratory & digestive tract and is a suspected carcinogen, mutagen and mitotic poison [14].

Hence, the removal of these pollutants from wastewaters in an eco-friendly way stands as a present major research concern. Therefore, in the present study, we attempted to remove this model azo dye pollutant from the contaminated water using as-synthesized Mn^{2+}/Mg^{2+} bimetal doped TiO_2 nanocatalysts and their photocatalytic efficiency was tested by optimizing the important reaction parameters like dopant concentration, surfactant concentration, pH, catalyst dosage and initial concentration of the dye for the better water pollution abatement.

2. Experimental

2.1. Materials

All the chemicals used in this research were of reagent grade and used without any further purification. Titanium tetra-n-butoxide (Ti(OBu)$_4$), Manganese nitrate [Mn(NO$_3$)$_2$].6H$_2$O and Magnesium Nitrate [Mg(NO$_3$)$_2$].6H$_2$O purchased from E-Merck Germany were used as precursors of TiO$_2$, Mn and Mg respectively, for preparing Mn^{2+}/Mg^{2+} bimetal doped TiO$_2$ samples. For the surfactant-assisted bimetal doped TiO$_2$ catalysts, 1,4-butane sultone obtained from Sigma Aldrich (Germany) was used. Methyl red (High media, India.) was used as a model azo dye pollutant for photocatalytic degradation studies. Milli-Q water used for the preparation of all the solutions.

2.2. Synthesis of nanocatalyst

Manganese and Magnesium bimetal ions doped nanotitania and Gemini surfactant-assisted Mn^{2+}/Mg^{2+} bimetal doped TiO$_2$ samples were prepared by sol-gel method. In this method, titanium tetra-n-butoxide (10 mL) was added to ethanol (20 mL) and acidified with 1.4 mL of HNO$_3$ taken in a pyrex glass vessel (Solution-I) and stirred for 20 min. Desired wt% (0.25-1.0 wt%) of Mn^{2+} and Mg^{2+} dopants proportionate to TiO$_2$ weight were taken in ethanol (20 mL) in another beaker and added 4.5 mL of Milli-Q water for effective hydrolysis purpose (Solution-II). Then the solution-II was slowly added to solution-I dropwise with continuous stirring. A colloidal solution that formed after complete mixing is further stirred for 90 min and aged for 48 h to obtain the gel. The formed gel was dried (at 70 °C), ground and calcined at 450 °C for about 5 h in a furnace. To get homogeneous powder the calcined samples were well ground after cooling.

To optimize the best dopant concentrations, the photocatalytic efficiency of the as-synthesized bimetal doped TiO$_2$ samples were tested by degrading Methyl red dye and 0.25 wt% Mn^{2+} and 1.00 wt% Mg^{2+} doped TiO$_2$ (MMT5) was found to be the best. For further enhancement in the photocatalytic activity of the MMT5 catalyst, Gemini surfactant-assisted MMT5 nanocatalysts were synthesized by following the same procedure but different wt% (5 wt%, 10 wt% and 15 wt%) of Gemini surfactant was added after the mixing of solution-I and solution-II. To study and compare the effect of dopants and surfactant on the photocatalytic properties of bimetal doped TiO$_2$, an undoped TiO$_2$ sample was prepared using the same procedure without adding dopants and surfactant precursors. Details of all the synthesized catalysts are presented in Table.1.

Table 1 Name assigned to different TiO$_2$ nanocatalyst samples

S.No.	Weight percentages of dopants (wt%)		Gemini Surfactant wt%	Name given to the Sample
1.	0.25 Mn	0.75 Mg	-	MMT1
2.	0.75 Mn	0.25 Mg	-	MMT2
3.	0.50 Mn	0.50 Mg	-	MMT3
4.	1.00 Mn	0.25 Mg	-	MMT4
5.	0.25 Mn	1.00 Mg	-	MMT5
6.	0.25 Mn	1.00 Mg	5	MMT5-GS1
7.	0.25 Mn	1.00 Mg	10	MMT5-GS2
8.	0.25 Mn	1.00 Mg	15	MMT5-GS3
9.	NIL		-	Undoped TiO_2

2.3. Characterization techniques

The crystalline structure of photocatalysts was studied by powder X-ray diffraction (XRD) spectra using PANanalyticaldifractometer with CuKα radiation (λ=0.15405 nm) operated

at 45 kV, 40 mA and 0.2 scan rate. Based on the Scherrer equation using full width at half maximum (FWHM), the crystallite size of TiO_2 nanocatalysts was determined. The UV-Visible Diffuse reflectance spectra (UV-vis DRS) of the catalysts were recorded in the range of 200-800 nm with a Shimadzu 3600 UV-Visible-DRS Spectrophotometer using $BaSO_4$ as reference. Scanning electron microscopy (SEM) JSM 6300, Japan equipped with energy dispersive X-Ray (EDX) spectroscopy was used to investigate the surface morphology and elemental analysis, respectively. The microstructure and particle size of the samples were analyzed by high-resolution transmission electron microscopy (HRTEM) JEM-2100 JEOL at an operating voltage of 200 kV. Fourier transform infrared spectra (FT-IR) of the nanocatalysts were recorded on an FT-IR spectrometer (Nicolet Avatar360). Brunauer- Emmet-Teller (BET) surface area, pore size and pore volume of the nanocatalysts were determined using Quanta Chrome Nova 2200E system by recording N_2 adsorption-desorption isotherms at 77.3 k. Photoluminescence (PL) analysis was performed by Hitchi F-7000 fluorescence spectrophotometer. The pH of the reaction mixture and the amount of MR degraded during the photocatalytic process were adjusted and monitored using Elico Digital pH meter (Model IIIE, EI) and UV−vis spectrophotometer (Shimadzu 1601), respectively.

2.4. Experimental procedure for the determination of visible light photocatalytic activity of nanocatalyst

The photocatalytic activity of surfactant-assisted Mn^{2+}/Mg^{2+} bimetal ions doped TiO_2 nanocatlyst was examined by the degradation of a model azo dye pollutant, Methyl Red in a previously reported visible

light photoreactor [15]. For visible light illumination, a high-pressure metal halide lamp (400 W, 35,000 lm, 436-546 nm output) has been used and placed 20 cm away from the pyrex glass vessel containing 100 mL of MR dye solution of desired concentration (1-10 mgL^{-1}) with sufficient amount of the catalyst. To screen the IR effect and to keep the constant temperature (25 °C) during the degradation experiments, water was passed continuously around the reaction vessel. Prior to visible light irradiation, the pH of the reaction mixture was adjusted to a desired value by addition of 0.1 N NaOH/0.1 N HCl and the reaction mixture was stirred in dark for 30 min to establish the adsorption-desorption equilibrium between MR dye and surface of the catalyst [16]. After the visible light irradiation, 5 mL aliquots of samples were collected at regular time intervals using Millipore syringe (0.45 μm) and change in the concentration of MR dye during the degradation process was studied with a UV−vis spectrophotometer (Shimadzu 1601) by measuring its absorbance at 525 nm. The percentage degradation of MR was determined by using the Eq. (1) [17]. (see Equation 1 in the Supplementary Files)

Where C_0 is the initial concentration of MR dye solution before degradation and C_t is the concentration at time t. For better photocatalytic degradation, the effect of reaction parameters like concentration of dopants, surfactant concentration, pH of the solution, catalyst dosage and initial dye concentration was studied and optimized by varying the measured parameter while keeping other parameters constant and the results are discussed in section 4.1-4.5. As the photocatalytic degradation of organic pollutants is mainly initiated by highly oxidative OH radicals, which can be easily captured by fluorescent probe molecules, the formation of •OH in the photocatalysis process was studied by photoluminescence (PL) technique using coumarin as a probe molecule [17].

3. Results And Discussion

3.1. X-ray Diffraction Study

From the XRD patterns of all the synthesized catalysts shown in Fig. 1a & b, all samples including undoped TiO_2 calcined at 450 °C for 5 h showed the formation of anatase phase having characteristic high-intensity diffraction peak at 2θ = 25.3° along with other corresponding small diffraction peaks at 2θ values 37.9°, 48.05° and 54.1° that can be indexed to planes of (101), (004), (200) and (211) of anatase phase respectively (JCPDS No. 21-1272). No extra peak found at 2θ=27.8°, indicated that there is no formation of the rutile phase. As the ionic radii of Mn^{2+} (0.78Å) and Mg^{2+} (0.72Å) are closer to the ionic radii of Ti^{4+} (0.68 Å), Mn^{2+} and Mg^{2+} dopant metal ions were expected to substitute Ti^{4+} ions in TiO_2 matrix which is confirmed by the absence of any diffraction peaks related to Mn and Mg oxides or other compounds [18,19]. And it is also known that as the Mn^{2+} and Mg^{2+} are more electropositive, the electronic cloud in each TiO_2 might be loosely held, favoring the formation of less dense anatase phase [20]. The average crystallite sizes of the undoped, bimetal-doped (MMT) and surfactant-assisted co-doped (MMT-GS) catalysts were calculated based on the FWHM of the characteristic high intensified peak using Scherrer equation [1] (d = kλ / β Cos θ), where d is the average crystallite size, k is 0.9 (Scherrer constant), λ is 1.5406 Å (X-ray wavelength), β is the full width at half maximum (FWHM) and θ

is the diffraction angle and are tabulated in Table 2. From the table, the average crystallite size of the catalysts found to be ranging from 7.21-10.22 nm, 10.86-12.87 nm and 18.30 nm for surfactant-assisted co-doped (MMT-GS), bimetal doped (MMT) and undoped TiO_2 nanocatalysts, respectively. The substitutional doping of metal ions into the TiO_2 lattice inhibited the grain growth by formation of Ti−O−Mn and Ti-O-Mg due to which the crystallite size was decreased in MMT catalysts. Further decrease in crystallite size was observed for the catalyst prepared in presence of surfactant, MMT-GS, which can be attributed to the effective capping nature of the Gemini surfactant which controls the nucleation and minimizes the agglomeration of TiO_2 nanoparticles during synthesis process [21].

Table 2 Crystallite size, band gap energy and BET surface area of undoped TiO_2 and all bimetal doped and surfactant-assisted TiO_2 catalysts calcined at 450 °C.

S.No	Nanomaterials	Crystallite size (nm)	Bandgap energy (eV)	BET surface analysis		
				Surface area (m^2g^{-1})	Pore volume (cm^3g^{-1})	Pore size (nm)
1	Undoped TiO_2	18.30	3.20	64.09	0.22	10
2	MMT1	12.87	2.97	84.73	0.23	7.3
3	MMT2	12.05	2.83	83.66	0.22	7.2
4	MMT3	11.37	2.79	94.85	0.23	9.3
5	MMT4	11.74	2.75	91.36	0.24	8.1
6	MMT5	10.86	2.68	112.03	0.24	7.0
7	MMT5-GS1	10.22	2.76	140.61	0.24	7.3
8	MMT5-GS2	7.21	2.66	230.20	0.25	6.4
9	MMT5-GS3	8.33	2.83	160.14	0.22	8.3

3.2. UV-Visible Diffuse Reflectance Spectra Study

From the UV-visible diffuse reflectance spectra of the undoped TiO_2, MMT and MMT-GS nanomaterials shown in Fig. 2a, it is observed that absorbance bands are shifted more towards the higher wavelengths i.e. red shifted in MMT and MMT-GS catalysts compared to undoped TiO_2, which is possible due to the decreased bandgap by co-doping of Mn^{2+} and Mg^{2+} into the TiO_2 matrix. The decrease in bandgap can be ascribed to the joint effect of these two metal dopant ions (Mn^{2+} & Mg^{2+}) in MMT and MMT-GS system, where these formed the extra energy levels below the conduction band of TiO_2 and thus reduces the electron-hole recombination by trapping electrons and enhances the visible light absorbance. From Fig. 2b it is further confirmed by bandgap energies obtained for all the synthesized catalysts using Kubelka-Monk formalism and Tauc plot method [22]. The corresponding band gap energy values are presented in Table 2. From the table, it is found that the average band gap values of the photocatalysts are in the range of 2.66-2.83, 2.68-2.97 and 3.20 eV for MMT-GS, MMT and undoped TiO_2, respectively. These outcomes revealed that all MMT and MMT-GS catalysts are visible light active and can be used as better photocatalysts. The catalysts MMT5, MMT5-GS1, MMT5-GS2 and MMT5-GS3 have the same

weight percentage of Mn and Mg; consequently, they have the absorption peaks nearly at the same wavelength. But in particular, among all the MMT's and GS assisted bimetal doped catalysts, MMT5-GS2 showed least bandgap energy i.e. 2.66 eV.

Before proceeds to further characterization, we have conducted trial photocatalytic degradation experiments for all the synthesized catalysts using MR dye. From the results it was noticed that among all the bimetal doped TiO_2 catalysts, 0.25 wt% Mn^{2+} & 1.00 wt% Mg^{2+} bimetal doped TiO_2 (MMT5) exhibited better photocatalytic activity and moreover MMT5 assisted with 10 wt% of GS, MMT5-GS2 has shown some more enhanced photocatalytic activity. Hence, we selected these two particular catalysts for further characterization with SEM-EDX, TEM, BET, FT-IR and photoluminescence study.

3.3. Scanning Electron Microscopy and Energy Dispersive X- ray Spectroscopy

The FESEM images shown in Fig. 3a, b and c illustrates the surface morphology of undoped TiO_2, MMT5 and MMT5-GS2, respectively. On comparison, it can be clearly seen that the morphology of the TiO_2 has been changed from large aggregates with a scratchy surface in undoped TiO_2 (Fig. 3a) to multiparticle agglomerated irregular shaped particles with rough surface in MMT5 and pseudospherical less agglomerated nanoparticles with smooth surface area and less particle size in MMT-GS2. This is clearly indicating that Mg^{2+} and Mn^{2+} bimetal ions doping and capping action with Gemini surfactant have a significant impact on the morphology of TiO_2 nanoparticles which controlled the grain growth and particle nucleation.

Also, the chemical composition of MMT5-GS2 sample was investigated by EDX and the results are depicted in Fig. 4. Along with the Ti and O elements of TiO_2, the dopant elements Mn and Mg are found in the spectra supports the presence of dopants in the TiO_2 matrix and there are no GS associated peaks are found in the spectra indicated complete elimination of GS after the calcination process. The quantitative analysis results are listed in a table inserted in Fig. 4 describes weight percentage as well as the atomic percentage of the compositional elements of the sample which indicates good compatibility with the dopant concentration used for the synthesis of TiO_2 nanoparticles.

3.4. Transmission Electron Microscope

The TEM images of MMT5 and MMT5-GS2 photocatalysts are shown in Fig. 5a and b respectively. The TEM image (Fig. 5a) of MMT-5 shows pseudospherical shaped with multiparticle agglomeration and an average particle size of 6.6 nm. Whereas in MMT5-GS2 (Fig. 5b), most of the TiO_2 particles are well dispersed with very low agglomeration compare to Fig. 5a and the particle size is in the range of 2.3-5.4 nm, with an average particle size of 3.8 nm. Thus, it clearly indicates that the GS was effectively inhibited the particle overgrowth and aggregation and resulted in less particle size with increased surface area, which is well correlated with BET results given in Table 2. The selected area electron diffraction (SAED) patterns shown in Fig. 5c confirmed the anatase phase with good crystallinity indexed by the concentric rings, which is in good agreement with XRD diffraction patterns. In addition to SAED, from the HR-TEM

image of MMT5-GS2 (Fig. 5d) the observed lattice fringes with d-spacing of 0.352 nm correspond to (101) plane of anatase and further confirms the single-crystal nature and high crystallinity of anatase TiO_2 [23].

3.5. Fourier Transform Infrared Spectroscopy

The incorporation of metal ion dopants, Mn^{2+} and Mg^{2+} into TiO_2 lattice was further confirmed by FT-IR results. The FT-IR spectra of the undoped TiO_2, MMT5 and MMT5-GS2 (before and after calcination) were shown in Fig. 6a-d. The peaks at 3403.01, 2926.10, 1616.36, 1383.78, 3378.14, 2918.69, 1626.67 and 1372.07 cm^{-1} corresponds to stretching vibrations of surface O-H and 3351.79, 2918.72, 1619.40 and 1383.80 cm^{-1} corresponds to the and bending vibrations of adsorbed H_2O molecules [24]. The stretching vibrations of Ti-O and bending vibrations of Ti-O-Ti observed at 575.41 and 1375.78 cm^{-1} in undoped TiO_2 (Fig. 6a) were deformed/shifted to 620.32 and 1300.12 cm^{-1} in MMT5 (Fig. 6b) and 540.01 and 1182.01 cm^{-1} in MMT5-GS2 (Fig. 6c & d) respectively, which can be attributed to the presence of dopants in TiO_2 lattice. Hence, the FT-IR study confirms that Mn^{2+} and Mg^{2+} are substitutionally doped into TiO_2 lattice by replacing Ti^{4+} and formed a new network i.e Ti-O-Mn and Ti-O-Mg which are in good agreement with the previous reports [25,26]. The FT-IR spectra of GS are shown in Fig. S1 as a supplementary file. The bands situated at about 2945.62, 1447.80, 1345.72, 1246.03, 1149.79, 1059.62 and 996.59 cm^{-1} in GS were shifted to 2855.77, 1734.95, 1459.87, 1206.73, 1136.50, 1094.06 and 982.86 cm^{-1} in MMT5-GS2 before calcination (BC) shown in Fig. 6c which confirms the existence of strong electrostatic interaction between GS and surface of catalyst in MMT5-GS2 before calcination [27].

From Fig. 6d, the absence of these peaks confirms that there was no surfactant remained in the synthesized catalyst, MMT5-GS2 after calcination (AC). This indicated that due to calcination at 450 °C, the surfactant is completely eliminated from nanocatalyst.

3.6. Brunauer-Emmett-Teller surface area analysis

To study the effect of bimetal doping and GS on the surface area and porosity nature of the as-synthesized TiO_2 nanoparticles of undoped TiO_2, MMT5 and MMT5-GS2, N_2 adsorption-desorption isotherms and their corresponding Berret- Johner- Halenda (BJH) pore size distribution plots were recorded and presented in Fig. 7a-b. From Fig. 7a, it results in a type -IV isotherm with H_2 hysteresis loop, characteristic of the ordered mesoporous structure of the catalyst [28]. The average surface area, A_{BET} (m^{2}g^{-1}) of all prepared catalysts was determined and tabulated in Table 2.

From Table 2 the MMT has shown increased surface area (112.03 m^{2}g^{-1}) compared to undoped TiO_2 (64.09 m^{2}g^{-1}) due to crystal growth suppression by dopants. Whereas catalyst prepared in the presence of GS surfactant, MMT5-GS2 showed higher surface area (230.20 m^{2}g^{-1}) compared to both MMT5 and undoped TiO_2. It could be strong evidence for the decreased particle size of the TiO_2 resulted from the effective capping ability of the surfactant, which restricts the particle growth and nucleation during the

synthesis process. To better compare the effect of bimetal doping and capping of GS on as-synthesized TiO_2 nanoparticles over single Mn^{2+} and Mg^{2+} doped TiO_2, comparative results are tabulated by referencing Mn and Mg single doped literature reports in Table 3.

Table 3 Comparative study of Mn^{2+}, Mg^{2+} single doped and Mn^{2+}/Mg^{2+} bimetal doped TiO_2 nanocatalysts.

TiO_2 Catalyst	Bandgap Energy (eV)	Surface Area (m^2g^{-1})	Crystallite Size (nm)	Reference No.
Mn-TiO_2	2.98	93	21.8	[29]
Mg-TiO_2	2.92	48.5	20	[30]
Undoped TiO_2	3.2	64.09	18.3	Present work
MMT5	2.68	112.03	10.86	Present work
MMT5-GS2	2.66	230.20	7.21	Present work

3.7. Photoluminescence Spectra

One of the essential reactive species in the process of photocatalysis is hydroxyl radical (•OH) and is responsible for oxidation reactions. Because of the high reactivity and short life of hydroxyl radical, it is impossible for direct detection. To inspect the production of hydroxyl radicals from the catalyst during the photocatalysis reaction, photoluminescence technique has been adopted using coumarin as a fluorescent probe molecule, which on reaction with hydroxyl radicals yields the 7-hydroxy coumarin [17]. In this technique, 0.10 g of catalyst is dispersed in 100 mL of 10 ppm coumarin solution in acidic conditions and illuminated to visible light irradiation. Small aliquots of reaction solution samples were withdrawn for every 30 min, filtered and photoluminescence intensity was measured in the range of 350-600 nm with excitation fixed at a wavelength of 435 nm. It has been observed from Fig. 8 that in-between of 440-460 nm there exist photoluminescence spectra of the generated 7-hydroxy coumarine with maximum emission at 450 nm. A linear increase in photoluminescence intensity was observed with increasing irradiation time. However, in the absence of irradiation, no excitation was observed for the sample (0 min in Fig. 8).

From the above results, it could be understood that the number of hydroxyl radicals produced on the catalyst surface was directly proportional to the irradiation time. The results further assure that the synthesized nanomaterial showed the enhanced rate of formation of hydroxyl radicals under irradiation to visible light. This is due to the fact that the already formed photo holes in the valence band of bimetal doped TiO_2 could directly react with H_2O/OH^- to produce hydroxyl radical [31].

4. Evaluation Of Photocatalytic Activity Of Synthesized Mmt-gs Nanocatalysts By Degradation Of Methyl Red

Visible light assisted catalytic activity of the synthesized MMT-GS photocatalysts were evaluated by degradation of MR. For better photocatalytic degradation, the effect of reaction parameters like concentration of dopants, surfactant concentration, pH of the solution, catalyst dosage, and initial dye concentration was studied and optimized as follows.

4.1. Effect of Metal ion dopant (Mn^{2+} & Mg^{2+}) Concentration

In order to find out and optimize the best dopant concentration of bimetal doped photocatalyst among all the synthesized MMT photocatalysts, degradation experiments were carried out with each photocatalyst under visible light irradiation by taking catalyst dosage 0.05 g, pH 4 and initial MR concentration 10 mgL^{-1}. The rate of degradation of MR has been studied by measuring the MR absorbance, which is inserted in Fig. 9. It can be seen from the figure that photocatalytic performance was found better for all the bimetal doped TiO_2 photocatalysts than undoped one and in specific among all the synthesized photocatalysts, the best catalytic performance was shown by 0.25 wt% of Mn^{2+} & 1.00 wt% of Mg^{2+} bimetal doped TiO_2, MMT5. This can be attributed to its narrowed bandgap resulted from the impurity energy levels between the valence band and conduction band that were created by the presence of both metal dopants which helps in the generation of more electron-hole pairs. And also, its less crystallite size and high surface area facilitate the adsorption of a greater number of dye molecules on its surface for the degradation [7]. Therefore, based on the above results MMT5 was selected for optimizing other parameters.

4.2. Effect of Gemini surfactant concentration

To find out the optimal concentration of GS in MMT5 photocatalyst for efficient photocatalytic performance, as synthesized MMT5-GS catalysts with various wt% of GS (5, 10 and 15 wt%) along with MMT5 were tested by the degradation of MR under visible light irradiation by maintaining other parameters constant i.e. catalyst dosage is 0.05 g, pH 4 and initial MR concentration 10 mgL^{-1}. It is observed from Fig.10 that all MMT5 nanocatalysts prepared in presence of GS degraded the MR in less time compared to MMT5 (Fig. 9) which clearly indicated the significant role of the capping nature of the GS on the photocatalytic activity of MMT catalysts. From the apparent rate constants obtained by slopes of the individual curves (inset of Fig. 10) it can be clearly seen that the degradation rate was increased up to 10 wt% GS concentration and then decreased on further loading. It could be due to the fact that increased GS concentration may restrict the effective doping of the metal ions into TiO_2 crystal lattice. Hence, MMT5-GS2 i.e.0.25 wt % Mn^{2+} & 1.00 wt % Mg^{2+} at 10 wt% of Gemini surfactant had been taken as a catalyst for further studies.

4.3. Effect of pH

According to Tang et al., [32] for charged substrates like TiO_2, there is a significant dependency on the pH value for the effective photocatalytic degradation, because the overall surface charge and adsorptive properties of TiO_2 nanomaterial depend strongly on solution pH. Hence, in this study the effect of pH on the catalytic performance of the MMT5-GS2 was carried out by ranging the pH from 2 to 8 and keeping

other parameters constant i.e. catalyst dosage 0.1 g and initial dye concentration 10 mgL^{-1}. From Fig. 11 it was observed that the degradation of MR is high in the acidic medium compared to the basic medium. This may be due to the strong electrostatic interaction between the positively charged surface (H$^+$ ions) of the catalyst and negatively charged dye molecules. When the pH increased to basic medium the catalyst surface acquires negative charge and electrostatically repels the like-charged dye molecules. In specific, the degradation of MR was high at pH 4, because as the positive charge (H$^+$ ions) on TiO$_2$ surface increases, negatively charged MR can easily be adsorbed on the surface of the catalyst. And a further increase in pH greater than 4 will facilitate the hydrolysis of metal ions on the surface of TiO$_2$ which seizes its photocatalytic activity.

4.4. Effect of Catalyst dosage:

To avoid the wastage of catalyst and minimize the screening effect, a number of experiments were carried out to get the optimum photocatalyst dosage by varying its amount ranging from 0.025 to 0.1 g using 10 mgL^{-1} of 100 mL of MR solution at pH 4. It was observed from Fig. 12 that the degradation of the dye increased linearly with the increase of catalyst loading up to 0.05 g because of the increased total surface area for dye adsorption. But after increasing the photocatalyst beyond 0.05 g, it creates turbidity and agglomeration of the catalyst particles due to excess photocatalyst and reduces the light transmission through the solution which leads to less photocatalytic activity [33]. And also, collisions between active molecules and ground-state molecules of bimetal doped TiO$_2$ results in deactivation of the catalyst particles [17].

4.5. Effect of initial concentration of dye

To study the effect of the initial concentration of dye at a fixed weight of catalyst (0.05 g) and pH 4, the experiments were carried out with different concentrations of MR dye from 5 to 15 mgL^{-1} and results are presented in Fig. 13. The results demonstrate that the rate of degradation of MR dye increased up to 10 mgL^{-1}. But, further increase in dye concentration causes deactivation of the catalyst due to the blanket effect [34]. And because of fixed catalyst dosage (0.05 g) there is no possibility to produce a sufficient number of OH radicles to counteract the increased number of dye molecules. Hence, the rate of degradation decreases.

5. Conclusions

Gemini surfactant abetted mesoporous Mn^{2+}/Mg^{2+} bimetal doped TiO$_2$ nanocatalysts were successfully synthesized by the sol-gel method without change in the crystallinity of TiO$_2$ nanoparticles. The effective charge separation and narrowed band gap created by Mn^{2+}/Mg^{2+} bimetal ions doping and reduced particle size and increased surface area resulted from capping of GS had significantly enhanced the photocatalytic performance of MMT5-GS2 nanocatalyst towards the degradation of MR dye under visible light irradiation. The photoluminescence results exhibited that OH radicals are the crucial reactive species

responsible for oxidative photocatalytic degradation of MR. The highest degradation of MR was achieved in 60 min at optimized reaction conditions of 10 wt% GS on 0.25 wt% Mn^{2+} / 1.00 wt% Mg^{2+} bimetal ions doped TiO_2, solution pH 4, catalyst loading of 0.05 g and initial MR concentration 10 mgL^{-1}. Based on its effective photocatalytic activity, MMT5-GS2 nanocatalyst could be used as a promising material for the abatement of water pollution caused by organic dyes.

Abbreviations

XRD: X-ray Diffraction, SEM: Scanning Electron Microscopy, EDX: Energy Dispersive X-ray Spectroscopy, FT-IR: Fourier Transform Infrared Spectroscopy, UV Vis-DRS: UV-Visible Diffused Reflectance Spectroscopy, TEM: Transmission Electron Microscopy, BET: Brunauer-Emmett-Teller surface area analyzer, PL: Photoluminescence Spectroscopy.

Declarations

Availability of data and materials

All data generated or analyzed during this study are included in this published article [and its supplementary information files].

Competing interests

The authors declare that they have no competing interests

Funding

Not Applicable

Authors' contributions

SRM: Conceptualization; Data curation; Formal analysis; Investigation, Methodology; Software; Writing original draft.

TSR: Supervision; Conceptualization; Methodology; Resources; Writing Original draft

IMR: Data curation; Formal Analysis; Software; Writing original draft; Review & editing.

SAA, GJ and MLVPC: Methodology; Formal Analysis; Data curation.

Acknowledgments

Not Applicable

References

1. Zhuyi W, Cheng C, Fengqing W, Bo Z, Meng Z, Jinxing W, et al. Photodegradation of rhodamine B under visible light by bimetal codoped TiO_2 J Hazard Mater. 2019;164:615-20.

2. Manjakuppam M, Venkatanarasimha RC, Raj KD, Ardhendu SG, Animes KG. Evaluation of bimetal doped TiO_2 in dye fragmentation and its comparison to mono-metal doped and bare catalysts. Appl Surf Sci. 2016;368:316-24.

3. Chelli VR, Golder AK. Bimetal doping on TiO_2 for photocatalytic water treatment: A green route. Europ Water. 2017;58:53-60.

4. Yaqin W, Ruirui Z, Jianbao L, Liangliang L, Shiwei L. First-principles study on transition metal-doped anatase TiO_2. Nano Res Lett. 2014;9:46.

5. Divya LKV, Siva RT, Swathi PJ, Manga RI, Abdul ASK, Kalyani P. Visible light driven mesoporous Mn and S co-doped TiO2 nano material: Characterization and applications in photocatalytic degradation of indigo carmine dye and antibacterial activity. Environ Nanotech, Monit & Manage 2018;10:494-504.

6. Zhang C, Chen S, Mo L, Huang Y, Tian H, Hu L, et al. Charge Recombination and Band-Edge Shift in the Dye-Sensitized Mg^{2+}-Doped TiO_2Solar Cells. J Phys Chem C. 2011;115:16418-24.

7. Desta SM, Matangi RC, Tirukkovalluri SR, Sreedhar B. Synthesis, characterization and visible light photocatalytic activity of Mg^{2+} and Zr^{4+} co-doped TiO_2 nanomaterial for degradation of methylene blue. J Asian Ceram Soc. 2017;5:136-43.

8. Sofianou MV, Tassi M, Boukos N, Thanos S, Vaimakis T, Yu J, et al. Solvothermal synthesis and photocatalytic performance of Mg^{2+}-doped anatase nanocrystals with exposed {0 0 1} facets. Catal Today. 2014;230:125-30.

9. RadhaDC, Siva RT. Synthesis of cobalt doped titania nano material assisted by gemini surfactant: Characterization and application in degradation of Acid Red under visible light irradiation. S Afr J Chem Eng. 2017;24:183-95.

10. Akpan UG, Hameed BH. The advancements in solgel method of doped-TiO_2 Appl Catal A: Gen. 2010;375:1-11.

11. Ikhmayies SJ. Characterization of nanomaterials. JOM. 2014;66:28-9.

12. Buitron CL, Quezada M, Moreno G. Aerobic degradation of the azo dye acid red 151 in a sequencing batch biofilter. Bioresour Technol. 2004;92:143-9.

13. Lachheb H, Puzenat E, Houas A, Ksibi M, Elaloui E, Guillard C, et al. Photocatalytic degradation of various types of dyes (Alizarin S, Crocein Orange G, Methyl Red, Congo Red, Methylene Blue) in water by UV-irradiated titania. Appl Catal B: Environ. 2002;39:75-90.

14. Sahoo C, Gupta AK, Anjali P. Photocatalytic degradation of Methyl Red dye in aqueous solutions under UV irradiation using Ag^+ doped TiO_2. Desalination. 2005;181:91-100.

15. Wu JCS, Chen CH. A visible-light response vanadium-doped titania nanocatalyst by sol-gel method. J Photochem Photobiol A: Chem. 2004;163:509-15.

16. Divya LKV, Siva RT, Swathi PJ, Manga RI, Ravi KM. Structure, photocatalytic and antibacterial activity study of Mesoporous Ni and S co-doped TiO_2 nano material under visible light irradiation. Chin J Chem Eng. 2019;27:1630-41.

17. Imandi MR, Siva RT, Lakshmi KVD, Ravi CM, Swathi PJ, Divya G. Poly 3-Thenoic acid sensitized, Copper doped anatase/brookite TiO_2 nanohybrids for enhanced photocatalytic degradation of an organophosphorus pesticide. J Environ Chem Eng. 2019;7:103211.

18. Shannon RD. Revised effective ionic radii and systematic studies of interatomic distances in halides and chalcogenides. Acta Cryst A 1976;32:751-67.

19. Venkatachalam N, Palanichamy M, Murugesan V. Sol-gel preparation and characterization of alkaline earth metal doped nano TiO_2 efficient photocatalytic degradation of 4-chlorophenol. J Mol Catal A: chem. 2007;273:177-85.

20. Jeong ED, Pramod HB, Jang JS, Lee JS, Ok-Sang J, Chang H, et al. Hydrothermal synthesis of Cr and Fe co-doped TiO_2 nanoparticle photocatalyst. J Cera Proc Res. 2008;9(3):250-3.

21. Swathi PJ, Siva RT, Lakshmi KVD, Manga RI. Fabrication of hetero-structured mesoporours TiO_2-$SrTiO_3$ nanocomposite in presence of Gemini surfactant: Characterization and application in catalytic degradation of Acid Orange. J Environ Chem Eng. 2018;6:6457-67.

22. Ghobadi N. Band gap determination using absorption spectrum fitting procedure. Int Nano Lett 2013;3:2.

23. Jaiswal R, Patel N, Kothari DC, Miotello A. Improved visible light photocatalytic activity of TiO_2 co-doped with Vanadium and Nitrogen. Appl Catal B: Environ. 2012;126:47-54.

24. Venkatachalam N, Palanichamy M, Banumathi A, Murugesan V. Enhanced photocatalytic degradation of 4-chlorophenol by Zr^{4+} doped nano TiO_2. J Mol Catal A: Chem. 2007;266:158-65.

25. Desta SM, Ravi CM, Siva RT, Sreedhar B. Synthesis, characterization and visible light photocatalytic activity of Mg^{2+} and Zr^{4+} co-doped TiO_2 nanomaterial for degradation of methylene blue. J Asian Ceram Soc. 2017;5:136-43.

26. Nidhi S, Deepali S, Dhiraj S. Experimental and theoretical investigations of Mn-N-co-doped TiO_2 photocatalyst for visible light induced degradation of organic pollutants. J Mater Res Tech. 2019;8:3995-4009.

27. Radha DC, Siva RT. Synthesis of cobalt doped titania nano material assisted by gemini surfactant: Characterization and application in degradation of Acid Red under visible light irradiation. S Afr J Chem Eng. 2017;24:183-95.

28. Deng QR, Gao Y, Xia XH, Chen RS, Wan L, Shoa G. V and Ga co-doping effect on optical absorption properties of TiO_2 thin films. J Phy: Conf Ser. 2009;152:

29. Lenik M, Verhovek D. Hydrothermal synthesis of Mn-doped TiO_2 with a strongly suppressed photocatalytic activity. MTAEC9. 2018;52(4):411-6.

30. Behnajady MA, Alizade B, Modirshahla N. Synthesis of Mg-Doped TiO_2 nanoparticles under different conditions and its photocatalytic activity. Photochem Photobiol. 2011;87:1308-14.

31. Mohamed MM, Al-Esaimi MM. Characterization, adsorption and photocatalytic activity of vanadium-doped TiO_2 and sulfated TiO_2 (rutile) catalysts: Degradation of methylene blue dye. J. Mol Catal A: Chem. 2006;255:53-61.

32. Tang WZ, An H. UV/TiO_2 photocatalytic oxidation of commercial dyes in aqueous solutions. Chemosphere. 1995;31:4157-70.

33. Venkatachalam N, Palanichamy M, Murugesan V. Sol-gel preparation and characterization of alkaline-earth metal doped nano TiO_2: efficient photocatalytic degradation of 4-chlorophenol. J Mol Catal A: Chem. 2007;273:177-85.

34. Subramani K, Byrappa K, Ananda S, Lokanatha RK, Ranganathaiah C, Yoshimura M. Photocatalytic degradation of indigo carmine dye using TiO_2 impregnated activated carbon. Bull Mater Sci. 2007;30:37-41.

Figures
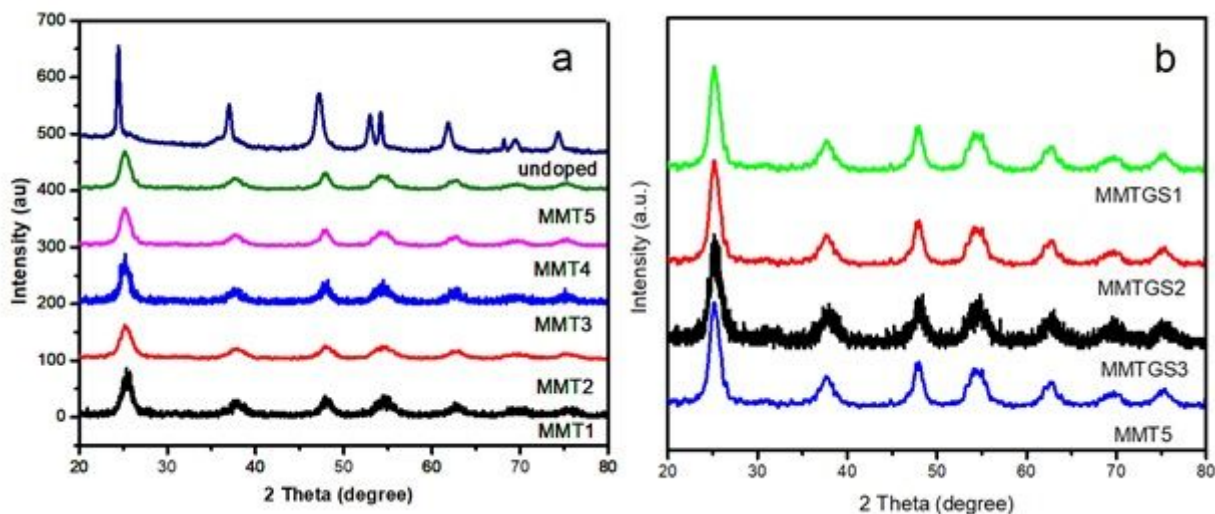
Figure 1

a XRD patterns of undoped TiO2 and Mn2+/Mg2+ bimetal doped TiO2 (MMT1-MMT5) catalysts. b MMT5 and Surfactant assisted catalysts (MMT5-GS1- MMT5-GS3).
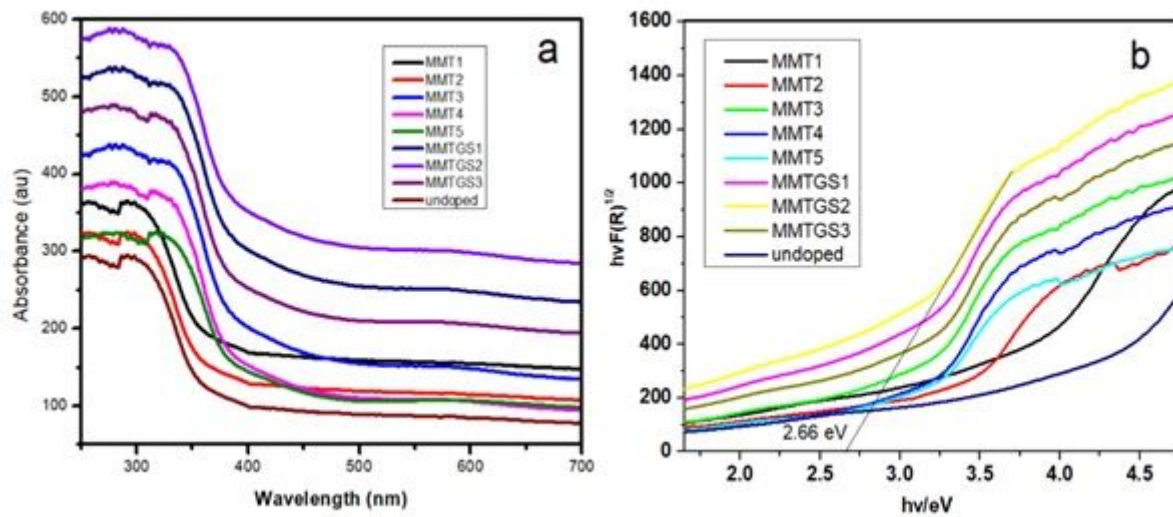
Figure 2

a UV-Vis DRS and b Kubelka-Munk formalism spectra of undoped TiO2, MMT and MMT5-GS catalysts.
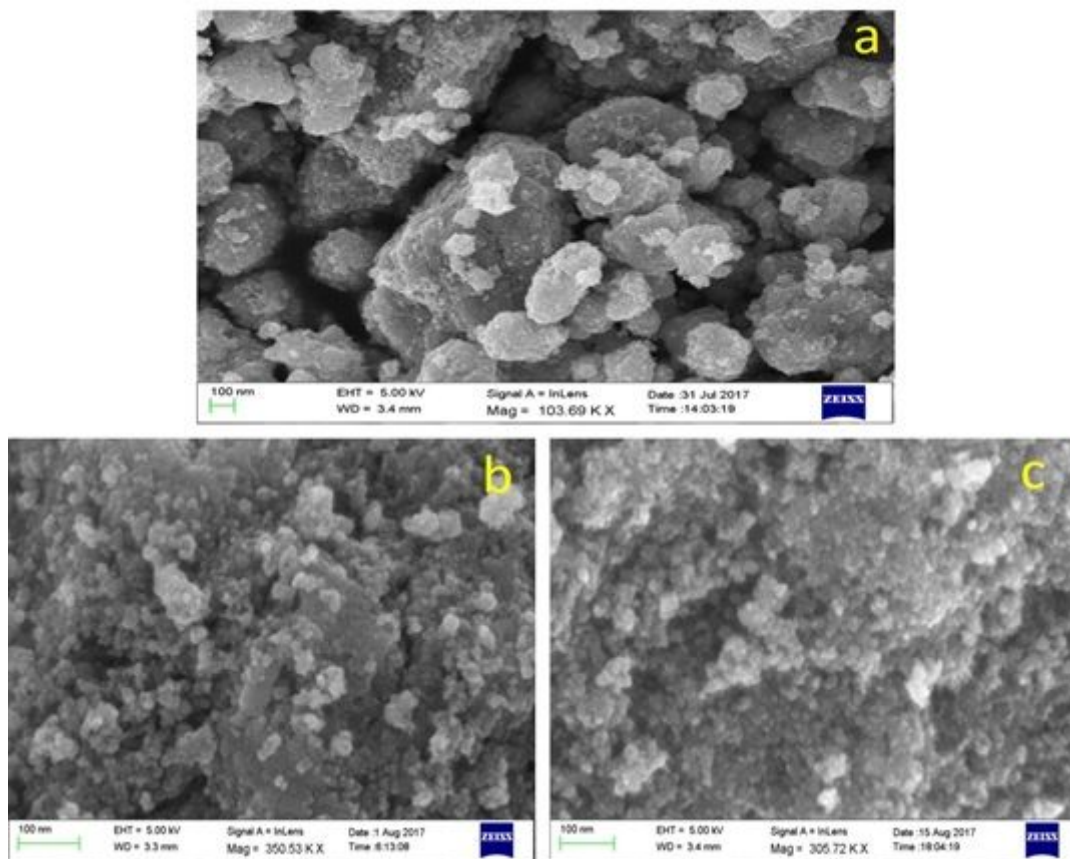
Figure 3

SEM micrographs of a Undoped TiO2, b MMT5 and c MMT5-GS2
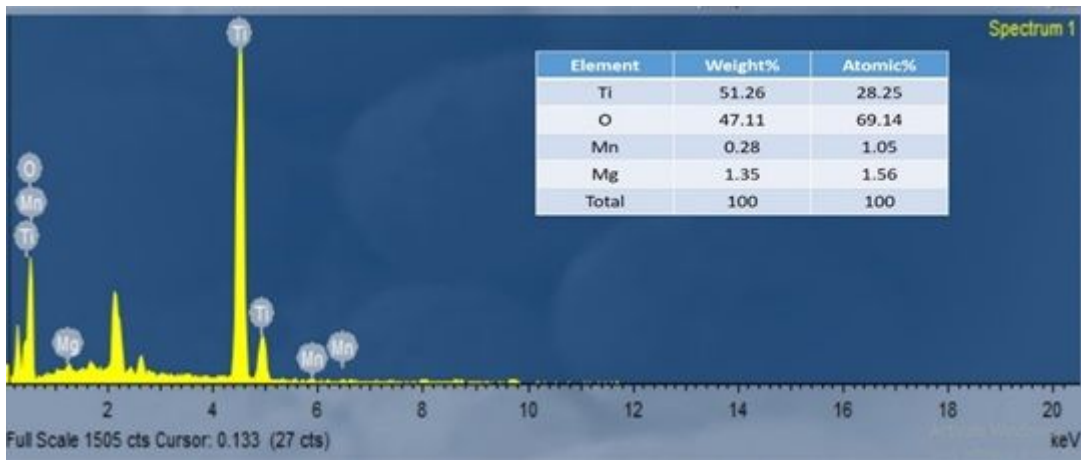
Figure 4

EDX spectrum of 0.25 wt% Mn2+& 1.00 wt% Mg2+ bimetal doped TiO2 in the presence of 10 wt% of surfactant (MMT5-GS2) after calcination.
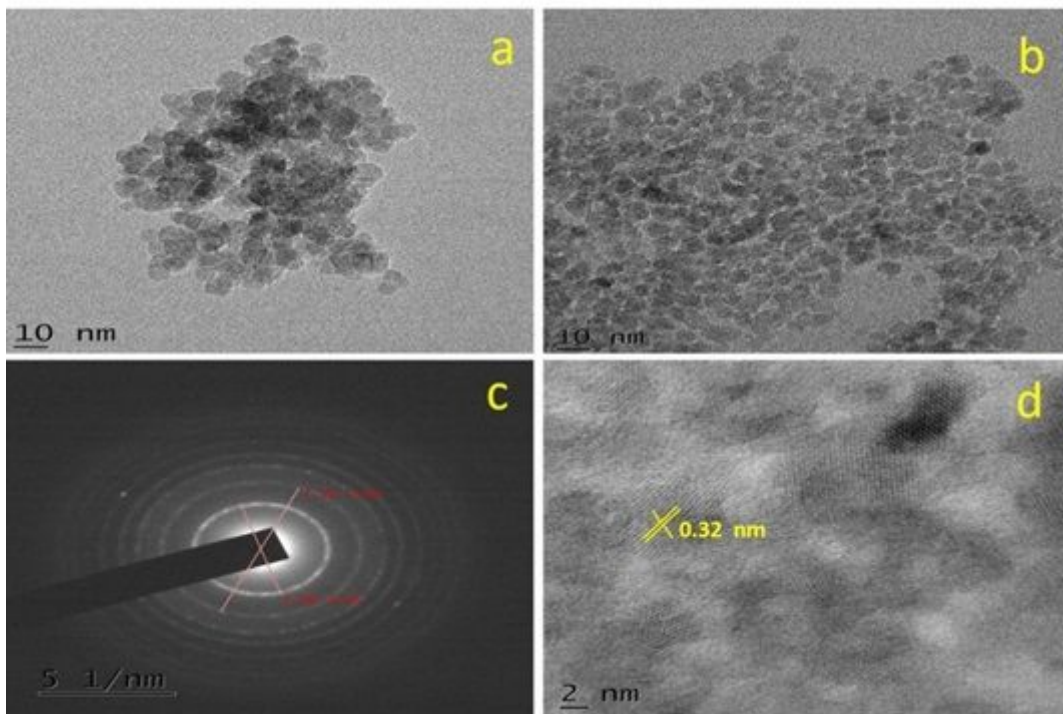
Figure 5

5 TEM image of a MMT5, b MMT5-GS2, c Selected area electron diffraction (SEAD) and d HRTEM Image of MMT5-GS2.
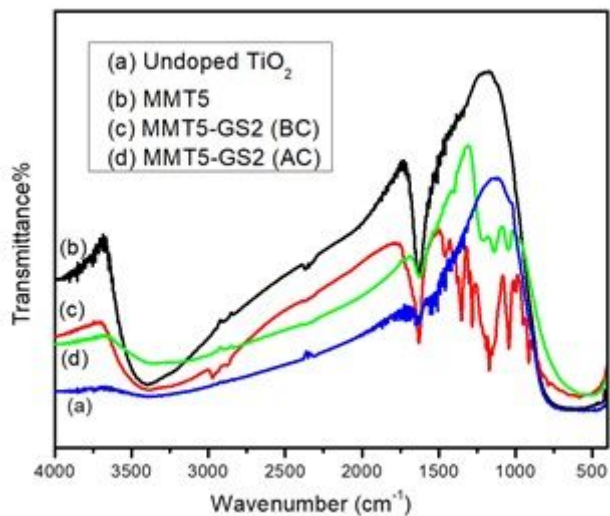
Figure 6

a FT-IR spectra of undoped TiO2, b MMT5, c MMT5-GS2 (BC), d FT-IR spectra of MMT5-GS2 (AC).
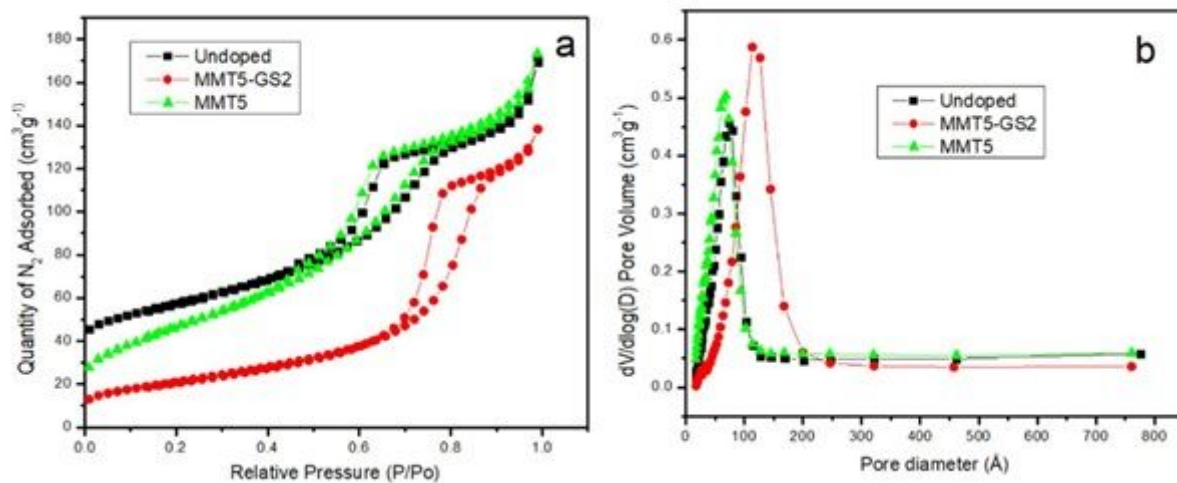
Figure 7

a N2 adsorption-desorption isotherm plot and b pore size distribution of undoped TiO2, MMT5 and MMT5-GS2.
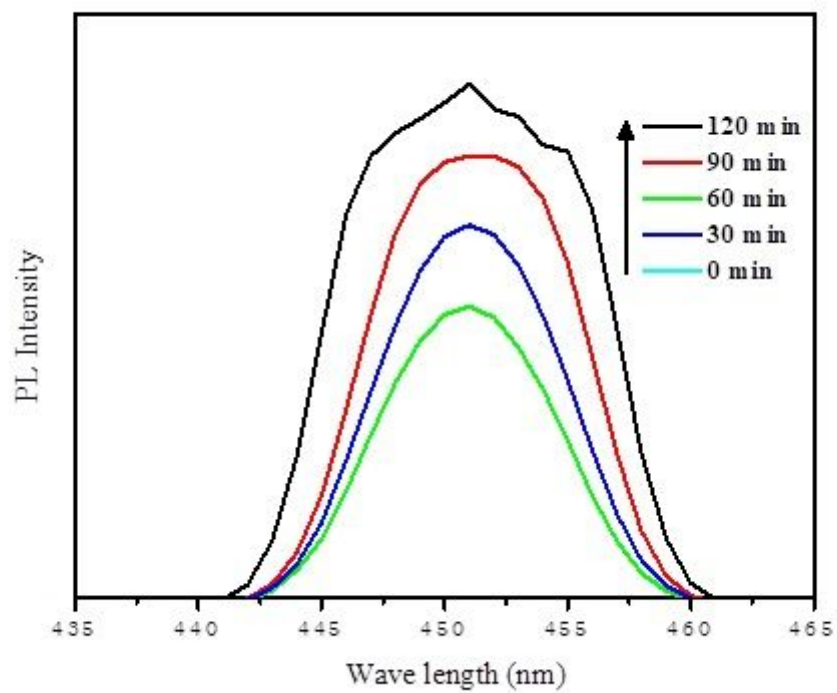
Figure 8

Photoluminescence spectra of MMT5-GS2
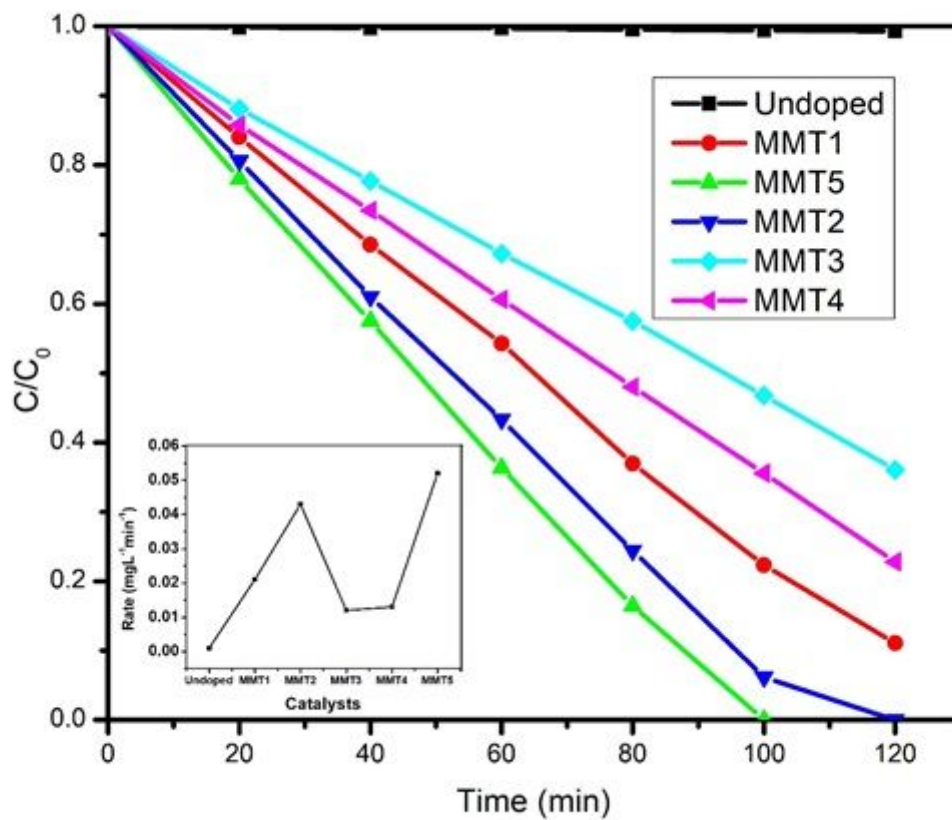
Figure 9

Effect of dopant concentration of bimetal doped TiO2 on photocatalytic degradation of MR dye. Here, catalyst dosage 0.05 g, pH 4 and [MR]= 10 mgL-1
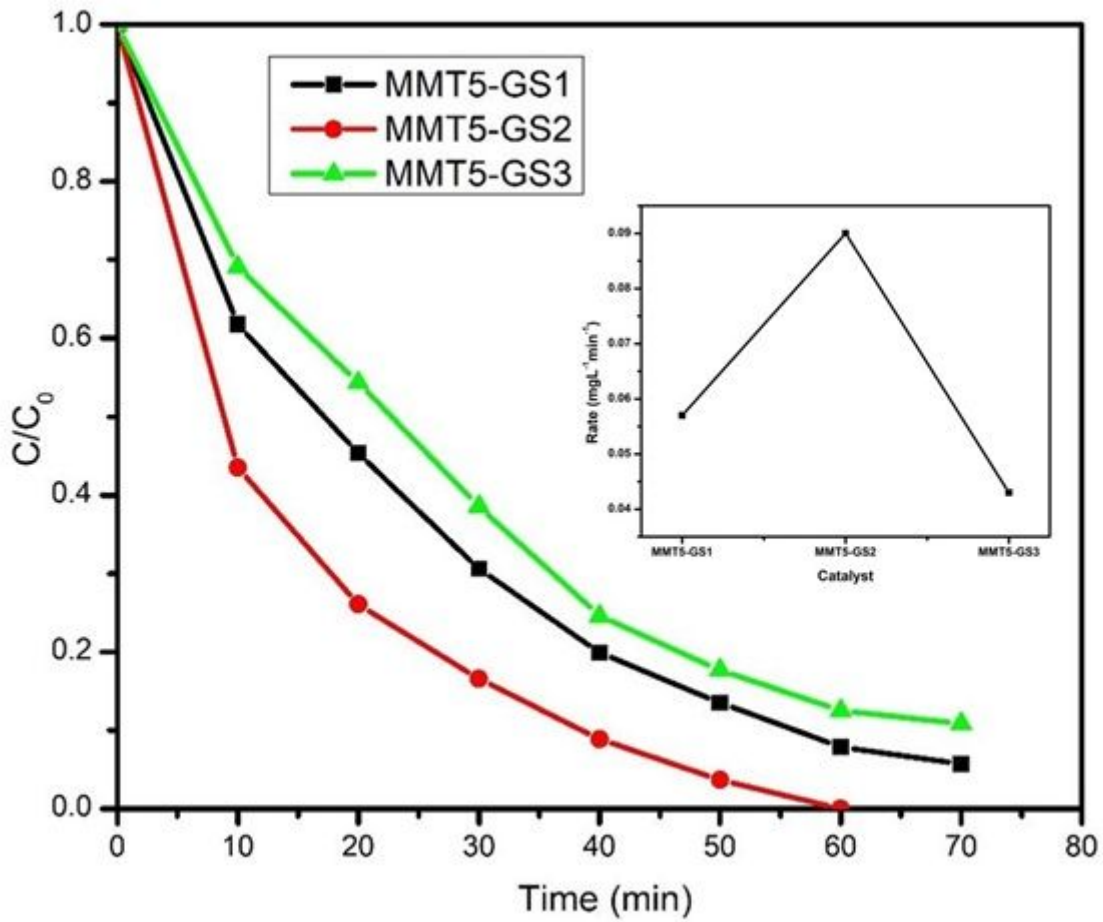
Figure 10

Effect of GS concentration on the photocatalytic activity of MMT5 on the degradation of MR. Here catalyst dosage is 0.05 g, pH 4 and [MR] = 10 mgL-1.
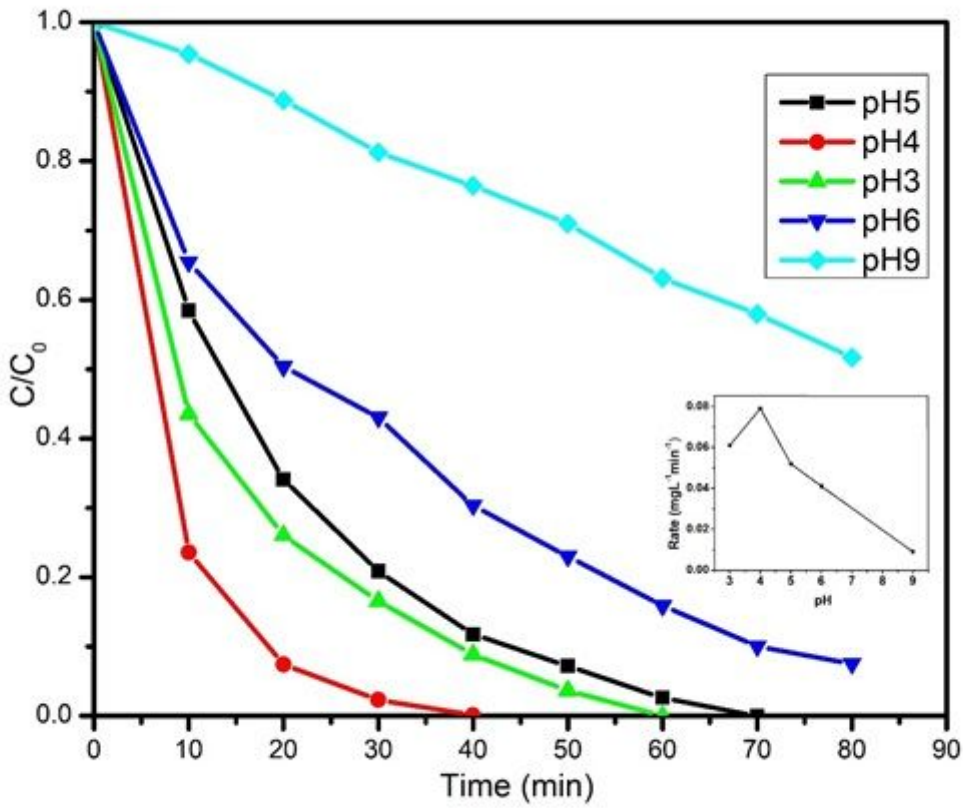
Figure 11

The effect of pH on the rate of degradation of MR dye by MMT5-GS2. Here, catalyst dosage 0.1 g and [MR]=10 mgL-1.
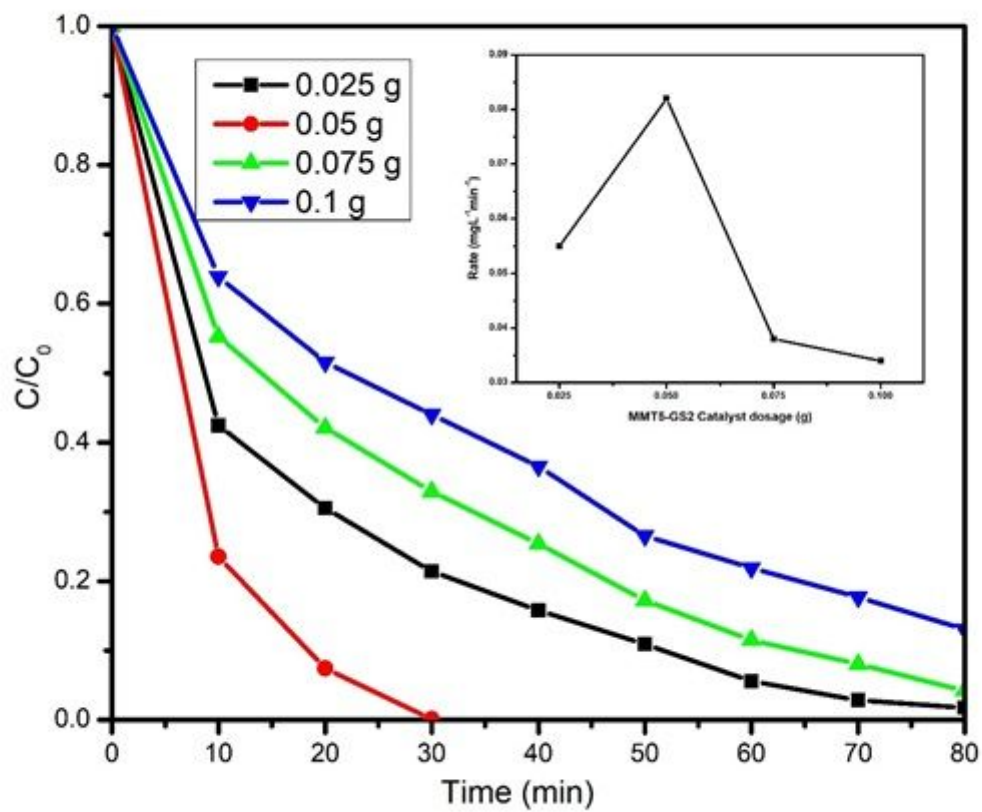
Figure 12

Effect of catalyst dosage on the degradation of MR by MMT5-GS2, here pH 4 and [MR] =10 mgL-1.
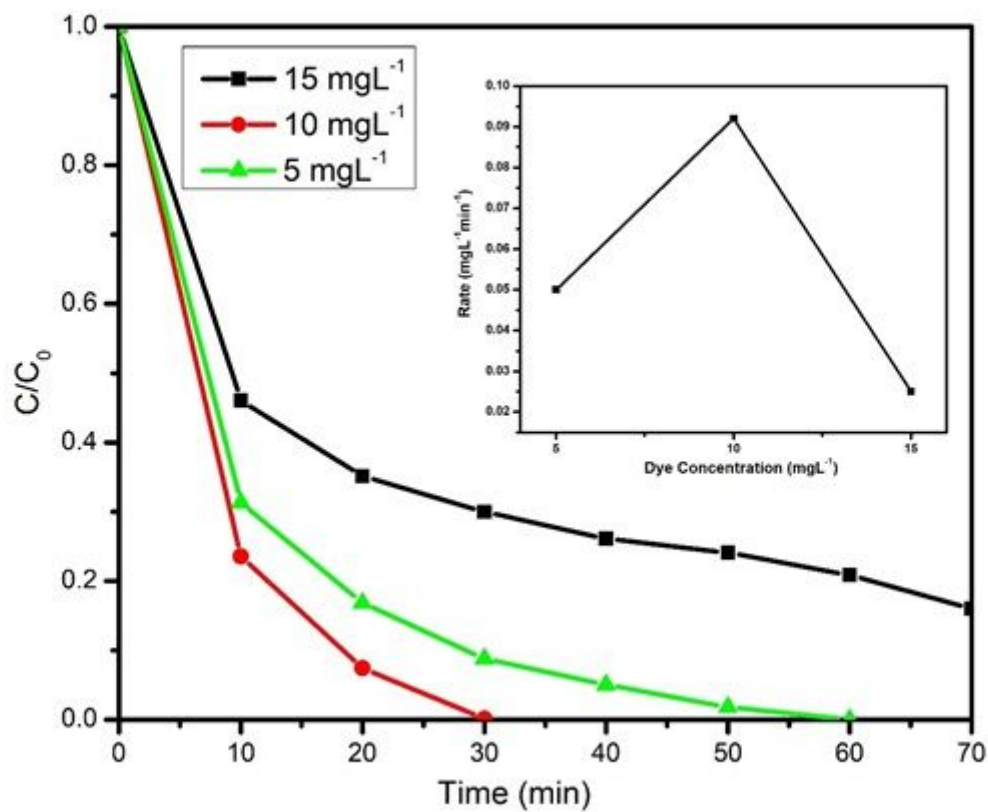
Figure 13

Effect of the initial concentration of the dye on the rate of degradation of MR dye by MMT5-GS2, here pH 4 and catalyst dosage 0.05 g.